Schweizerische Eidgenossenschaft
Confédération suisse
Confederazione Svizzera
Confederaziun svizra

Federal Department of the Environment, Transport, Energy and Communications DETEC

Swiss Federal Office of Energy SFOE
Energy Research and Cleantech Division

REEL Demo – Romande Energie ELectric network in local balance Demonstrator

Deliverable: 3f Assessment of investment costs of controllable batteries and comparison with grid refurbishment

Demo site: Chapelle

Developed by
Lorenzo Nespoli, ISAAC, SUPSI
Vasco Medici, ISAAC, SUPSI
Roman Rudel, ISAAC, SUPSI

[Canobbio, 30.03.2022]

University of Applied Sciences and Arts
of Southern Switzerland

SUPSI

Date: 30. March 2022

Place: Bern

Publisher:
Swiss Federal Office of Energy SFOE
Research Programme, Energy - Economy - Society (EES)
CH-3003 Bern
www.bfe.admin.ch
energieforschung@bfe.admin.ch

Agent:
University of Applied Sciences and Arts of Southern Switzerland (SUPSI)
Department for Environment Constructions and Design
Institute for Applied Sustainability to the Built Environment
Via Flora Ruchat-Roncati 15
CH-6850 Mendrisio
https://www.supsi.ch/isaac

Author:
Lorenzo Nespoli, ISAAC, SUPSI (lorenzo.nespoli@supsi.ch)
Vasco Medici, ISAAC, SUPSI (vasco.medici@supsi.ch)
Roman Rudel, ISAAC, SUPSI (roman.rudel@supsi.ch)

SFOE head of domain: Dr. Michael Moser, michael.moser@bfe.admin.ch
SFOE programme manager: Dr. Michael Moser, michael.moser@bfe.admin.ch
SFOE contract number: SI/501523

Contents

1 Summary

When properly operated, installing distributed electric storage in the low and medium voltage grid can be a method to avoid grid refurbishment, i.e. installing bigger cables and transformers. In this deliverable we have tried to quantify the avoided costs thanks to operating the two installed batteries in Chapelle-sur-Moudon in order to help the grid. One battery is privately owned, and as such its main goal is to reduce consumption costs, while the bigger battery is owned by the DSO and used solely to help decrease losses and reduce the power peak. The way the batteries are coordinated has been described in the deliverable 3d3 design and test of distributed DSM algorithms that use communication and new forecasting models). Here we analyzed the effect of these operations on the overall power profile at the LV/MV trafo during the pilot test period, and estimate the impact on cables and trafo degradation. Finally, we try to extrapolate the economic benefit of such decrease of degradation on the DSO total costs.

2 Background

3 Estimation of aging acceleration factors for cables and transformer

3.1 Cable degradation estimation

Cable degradation is mainly due to the degradation of the cable insulation. The main aging mechanisms are degradation due to high temperatures and due to electrical stress. The authors in (1) propose a multistress model, which can be expressed as:

$$\frac{L}{L_o} = \frac{L_1}{L_0}\frac{L_2}{L_o}\dots\frac{L_N}{L_0}G\left(S_1, S_2, \dots S_N\right) \tag{1}$$

where L is the life of the cable under multiple stresses and $L_1 ... L_N$ are single stress lives for stress S_1 ... S_N and G is a correction function taking into account that life under multiple stresses is usually higher than that derived by simple multiplicative laws. Since the single-stress electrical and temperature effects on cable life can be modeled be respectively modeled with an inverse power low

$$\frac{L_E}{L_0} = \left[\frac{E}{E_o}\right]^{-n} \tag{2}$$

and with a ratio of Arrhenius laws

$$\frac{L_T}{L_0} = \exp(-E_a T/R) \tag{3}$$

where E_a is the activation energy associated to the insulation material and R is the gas constant. The authors propose the following aging law:

$$\frac{L}{L_0} = \left[\frac{E}{E_o}\right]^{-(n-bT)} \exp(-BT) \tag{4}$$

However, the interaction between electrical and thermal aging is usually disregarded (see for example the International Atomic Energy Agency (IAEA) Cable Ageing technical report (2) and (3)). Furthermore, authors in (4) compared different aging models for cable insulations, and reported only a small different between models considering and disregarding the electrical field and temperature interaction. Therefore, we just considered temperature-induced degradation in the present study.

Insulator temperature computation Insulator temperature can be computed as a function of ambient temperature and the instantaneous cable's power. If the exact temperature at insulator-conductor interface is needed, an equivalent resistance coefficient must be used, which can be estimated starting from geometrical considerations on the cable stratigraphy and type of insulator used, as shown for example in (5). In this study we have used a simpler method, as suggested in (6), where the cable operating temperature is found by using the Joules loss formula and knowing the maximum operating power and its corresponding temperature:

$$T(t) = T_a(t) + (T_{max} - T_{ref}) \left(\frac{P(t)}{P_{max}} \right)^2 \tag{5}$$

where $T(t)$ and $T_a(t)$ are the cable operating temperature and the ambient temperature at the current time, T_{max} and T_{ref} are the maximum operating cable temperature and reference temperature (20 °C), while $P(t)$ and P_{max} are the current and maximum cable power. Equation 5 is then plugged into 3 to retrieve the power-dependant instantaneous degradation.

3.2 Transformer degradation estimation

Transformer degradation is mostly due to the operating temperature of the hot-spot winding of the transformer. The computation of this temperature is more complex than the computation of cables operating temperatures, as different source of heating must be taken into account. We considered an oil insulated transformer, and followed the procedure presented in (7) to compute the hot-spot temperature, θ_H. This temperature can be obtained as the summation of two thermal jumps:

$$\theta_H = \theta_A + \theta_{TO} + \theta_g \tag{6}$$

where θ_A is the ambient temperature, θ_{TO} is the relative oil temperature w.r.t. the ambient one, and θ_g is the conductor hot-spot temperature w.r.t. the oil.

$$\begin{aligned} \theta_{TO} &= \theta_{TO-R} \left(\frac{P_{LL} + P_{NL}}{P_{LL-R} + P_{NL}} \right)^{0.8} \\ \theta_g &= \theta_{g-R} \left(\frac{P_{DC} + P_{EC}}{P_{DC-R} + P_{EC-R}} \right)^{0.8} \end{aligned} \tag{7}$$

where θ_{TO-R} is the rated oil temperature rise with respect to the ambient temperature, θ_{g-R} is the rated conductor temperature rise relative to oil temperature and P_{DC-R}, P_{LL}, P_{EC-R} are the rated ohmic, load and eddy current losses respectively. These can then be expressed as a function of the transformers' load factor β:

$$\begin{cases} P_{LL} = P_{DC} + P_{EC} + P_{OSL} \\ P_{DC} = \beta^2 P_{DC-R} \\ P_{EC} = \beta^2 P_{EC-R} F_{HL} \\ P_{OSL} = \beta^2 P_{OSL-R} F_{HL-STR} \end{cases} \tag{8}$$

where:

$$\begin{aligned} P_{EC-R} &= 0.33 \left(P_{LL-R} - P_{DC-R} \right) \\ P_{OSL-R} &= 0.67 \left(P_{LL-R} - P_{DC-R} \right) \end{aligned} \tag{9}$$

$$P_{DC-R} = 3 \left(R_1 I_{R1}^2 + R_2 I_{R2}^2 \right) \tag{10}$$

The harmonic loss factor F_{HL} and the armonic loss factor for other stray losses F_{HL-STR} depend on the magnitude of the harmonic components of the current (the fundamental being 50 Hz),

Name	Type	Value	Description
T_t	var	-	Cable operating temperature at time t
$T_a(t)$	var	-	Ambient temperature at time t
T_{max}	param	95	Maximum operating temperature
P_{max}	param	250 kW	Maximum operating power
E_a	param	0.65 eV	Activation energy for XLPE cables
R	param	8.63e-5 eV/K	Gas constant
$B = E_a/R$	param	7540 K	Arrhenius law exponent for the cable
T_{ref}	param	15	Reference operating temperature for the cable

Table 1: Variables and parameters for the computation of the cable aging.

and can be computed with the following weighted average:

$$F_{HL} = \frac{1}{I^2}\sum_{k=0}^{N} k^2 I_k^2,$$
$$F_{HL-STR} = \frac{1}{I^2}\sum_{k=0}^{N} k^{0.8} I_k^2, \tag{11}$$
$$\beta = \frac{S}{S_R} \cong \frac{I}{I_{R2}}, I^2 = \sum_{k=0}^{N} I_k^2,$$

It must be noted that we do not possess harmonic measurements which need to compute the harmonic decomposition (and retrieve the coefficients k) neither the total harmonic distortion (THD) at the PCC, and the best we can do to approximate these losses is to guess the harmonic decomposition of the signal and take it constant between different approaches. This is not realistic, since the operations of the battery can alter the harmonics of the current. However, this uncertainty can be considered of second order when considering the exponential relation for the computation of the transformer aging, which is characterized by a larger exponent w.r.t. the one used for the computation of the cable aging. Also in this case, we use a ratio of Arrhenius laws to estimate the relative aging of the transformer w.r.t. different power profiles, as required by the IEEE standard C57.91™-2011 (8) to compute the transformer insulator life. Here θ_{Href} is the hot-spot reference temperature for which the transformer life is regarded to be the nominal one, and B is a constant set to 1500 by the C57.91 standard.

$$F_{AA} = \exp\left(\frac{B}{\theta_{Href} + 273} - \frac{B}{\theta_H + 273}\right) \tag{12}$$

This constant is much higher than the one we used to compute the aging of the power cable insulation, and results in a much more temperature-sensitive relation, as can be seen by comparing the last two rows of figure 1 and 3.

3.3 Numerical results from pilot

The presented methods to estimate the acceleration aging factors for the cables and the transformer have been applied to the data from the pilot in Chapelle. The data is relative to the 4 months period in which the batteries have been operated by SUPSI. Briefly speaking, the strategy tried to coordinate the two installed batteries to both minimize the costs for the privately owned battery and to perform peak shaving at the trafo, in a Pareto-optimal way.

Name	Type	Value	Description
θ_H	var	-	Hot-spot temperature of the transformer
θ_{Href}	param	95	Hot-spot ref. temperature of the transformer (8)(7)
θ_A	var	-	Ambient temperature
θ_{TO}	var	-	Oil temperature w.r.t. air
θ_g	var	-	Hot-spot temperature w.r.t. oil
P_{DC}	var	-	Ohmic losses
P_{DC-R}	var	-	Rated ohmic losses
P_{LL}	var	-	Load losses
P_{LL-R}	param	3.25 kW	Rated load losses
P_{EC}	var	-	Eddy current losses
P_{EC-R}	var	-	Rated eddy current losses
P_{OSL}	var	-	Other stray losses
P_{OSL-R}	var	-	Rated stray losses
P_{NL}	param	0.65 kW	No-load losses
$I_{R1} - I_{R1}$	var	-	Currents at the high-low voltage winding
$F_{HL} - F_{HL-STR}$	var	-	Harmonic loss factor - for stray losses
β	var	-	Load factor
S_R	param	250 kVA	Rated transformer power
$U_{R_1} - U_{R_2}$	param	20 - 0.4kV	Primary - secondary rated voltage
$R_1 - R_2$	param	10.4 - 0.00416 Ω	Per-phase DC resistance primary-secondary winding
S_R	param	-	250 kVA
S_R	param	-	250 kVA
S_R	param	-	250 kVA
S_R	param	-	250 kVA
B	param	15000	Arrhenius law exponent for the transforme (8)

Table 2: Variables and parameters for the computation of the transformer aging.

Since we have measurements for both the power at the trafo and batteries operations, we subtracted the effect of the batteries and performed what-if analysis. In particular, we compared the degradation under four cases:

1. A baseline, in which no batteries is installed. This was achieved subtracting batteries charging and discharging operations from the power measurements at the transformer.
2. The battery real operations, in which we have used the measured power at the transformer which actually occurred.
3. The case of ideal batteries. We subtracted the batteries operations and we then simulated two batteries with the same capacity and charging limits than the installed one, considering they can use perfect forecasts for the power at the transformer. Secondly, the ideal batteries has also perfect knowledge of their state of charge with no delay, which is not the case for the real batteries. This case is considered the lower bound of what can be achieved in terms of cable and trafo temperature decrease w.r.t. the baseline, and thus a lower bound for age reduction.
4. Ideal batteries with ramp constraint. This is the same of the previous case, but adding ramp constraints for the operated battery, restricting the power variations to 10 kW/min.

In figure 1 the key quantities for the computation of the cable degradation are shown for a period of three days. The top plot shows the power under the four aforementioned cases. The top plot shows the power at the trafo, the blue line indicating what would have happened without the batteries in place. The red line shows the resulting power under the real battery operations in the considered period. The batteries try to perform peak shaving flattening the overall consumption. During the first day we can see the batteries charge from the installed PV (when the trafo is injecting back into the MV grid) and then soon discharges themselves; this is likely due to forecasting errors overestimating the future consumption. The middle plot shows the cable's temperature obtained by equation (5), while the last plot shows the degradation factor computed from equation (3). It can be seen how even small deviations in the cable temperatures can result in high changes in the degradation factor, as expected. From the plot is clear that the battery operated in a peak-shaving mode has a high impact in reducing the cable temperature and, as a consequence, to increase the life of the cable. The effect of the real batteries on the aging fall in between the baseline case and the operation of ideal batteries with perfect knowledge on the future. The results on the total monitoring period are reported in table 3, as normalized averages of the acceleration factor. The first column report the relative improvement of lifespan over the base case, considering all the monitoring period. The second column consider just the periods for which the cable's temperature was above the reference operating temperature, which is the temperature for which the standard life of the cable is computed, and under which no life shortening can be considered, which in this case was fixed to 15 °C. The difference in terms of degradation between the ideal case and the ideal case with ramp constraints is negligible, while under the operation of the real battery the degradation reduction is roughly 62% the one of the ideal cases, when considering the filtered period using the reference temperature.

In figure 4 we reproduced the results from (7). The figure shows on the left the relation between the load factor of the trafo, β and the hot spot temperature computed by using equation (6), with a fixed ambient air of 30 °C. On the right plot the Arrhenius law for the aging factor is plotted in logarithmic scale. It can be notice how a small change in the load factor results in a sensitive change in the transformer's life; this is a more severe relationship w.r.t. the one occurring between the total power in the cable and its aging factor. This is mainly due to the different exponent in the Arrhenius law used to model the aging of the cable's insulation and the oil insulated transformer. The corresponding values used can be found in table 3 and 4 respectively. The increase effect in degradation can be seen comparing the last two rows of figure 3 and 1: the ratio between the degradation and operational temperature is clearly higher for the transformer. The results over the considered period are reported in table 4. When

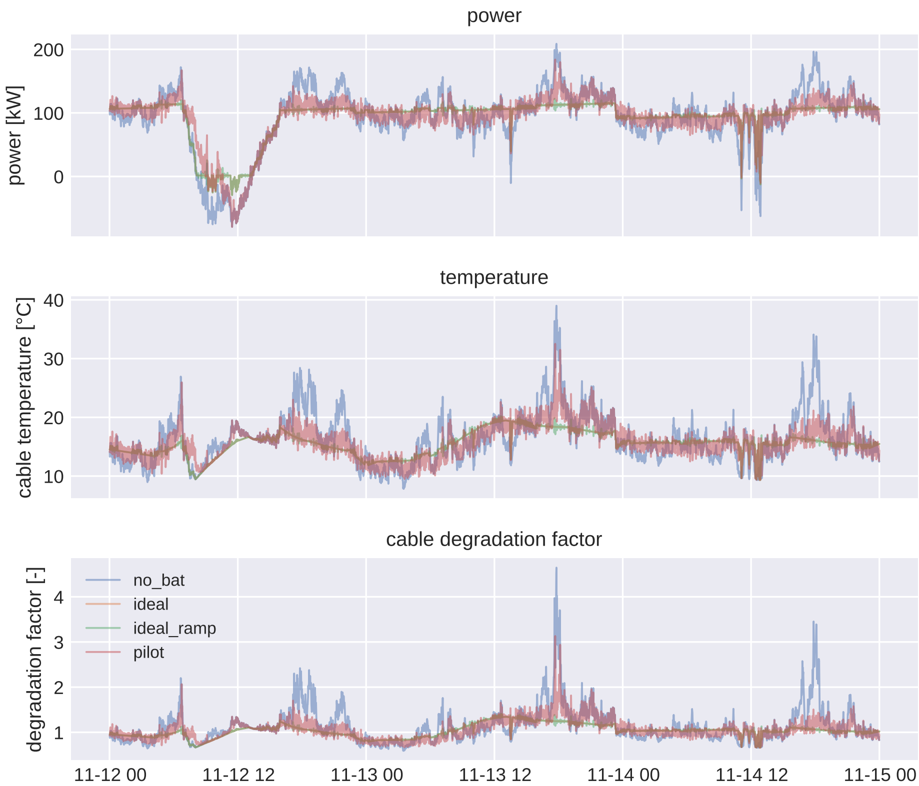

Figure 1: Example of time series for the computation of cable degradation. Top: instantaneous power for the PCC cable. Middle: corresponding cable temperature computed using equation (5). Bottom: degradation factor for the 4 considered cases, computed using equation (3)

considering the whole period, the average reduction in degradation is very high, going from 87% for the ideal battery to 52% for the pilot. However, a more realistic life increase can be computed when taking into account only the periods in which the operational temperature of the hot-spot goes above the reference temperature. In this case the average reduction in the degradation is 1.5 % for the ideal cases and 1% for the pilot.

	relative improvement	**relative improvement over T ref**
ideal	0.0659	0.08
ideal_ramp	0.0657	0.08
pilot	0.0394	0.05

Table 3: Reduction of cable degradation

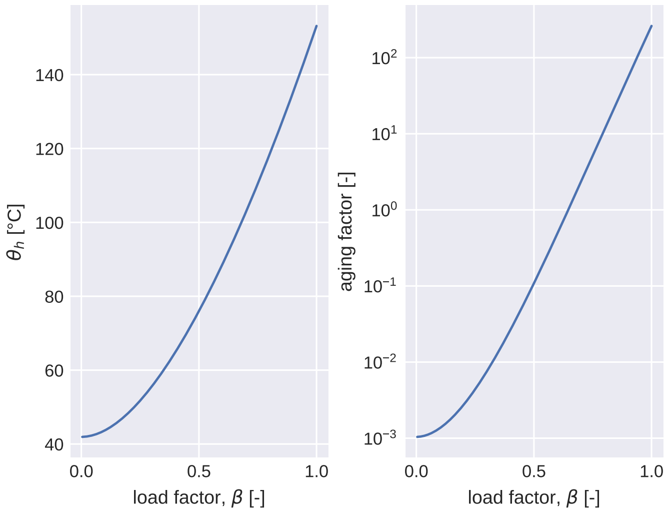

Figure 2: Hot-spot temperature and aging factor computed using equation (6) and (12) as a function of load factor, using the parameters of table 2 and a reference ambient temperature of 30 °C.

	relative improvement	**relative improvement over T ref**
ideal	0.870	0.015
ideal_ramp	0.869	0.015
pilot	0.528	0.01

Table 4: Reduction of transformer degradation

4 Cost estimation

4.1 Degradation

We can use the estimation over cables and transformer degradation reduction from table 3 and 4 to infer a total cost reduction induced by the battery operations. Considering a similar effect over the operating temperatures for all the lifespan of the cables and transformer, we can estimate an increase of lifespan in the range of 5-8% for the cables and 1-1.5% for the transformer. The cost for the labour and the three-phase copper cables was based on a consultation with AEM DSO, while the cost of transformers is based on the standard costs provided by the "Association des entreprises" électriques suisses AES + swisselectric" (2008) and the costs reported in (9). A realistic estimation of the main cables of the considered grid (including installation costs) is about 50k CHF (20 kCHF cables and 30 kCHF installation), while the cost for the 250 kVA transformer can be estimated around 16 kCHF with 50 kCHF of installation costs. It is reasonable to consider just the material costs for both. Under these assumptions, we can estimate a cost reduction between 1.16 kCHF and 9.1 kCHF, if considering degradation to start after the reference operating temperatures or degradation under all conditions, respectively.

4.2 Peak reduction

Performing peak shaving also reduces the costs due to the power peak tariff. This tariff is usually computed on the monthly maximum on a 15 minute basis. It is extremely challenging to

Figure 3: Example of time series for the computation of transformer degradation. Top: load factor. Middle: corresponding hot-spot winding temperature computed using equation (6). Bottom: degradation factor for the 4 considered cases, computed using equation (12)

optimize for this kind of tariff, since it is not possible to precisely forecast in advance when the monthly maximum consumption will be. In this sense, our optimization algorithm is only an heuristic for the reduction of monthly peak costs. We can however assess the monthly peak reduction for the controlled month and compare it with a perfect controller with perfect forecasts. Assuming a peak tariff of 6.96 CHF/kW/month, the cost reduction for the ideal and the actually controlled battery are reported in table 5. We can see how the real battery achieved less than 10% of the cost reduction achievable with the perfect knowledge of the monthly peak. A better performance could be possibly be achieved with a stochastic controller; however the use of a stochastic formulation in a multilevel setting is not straightforward. We further explore the performances achievable with a deterministic control by simulating n control system in parallel. Starting from the measurements from the pilot, with and without the battery operations, we sampled 30000 days for n parallel and identical systems. We then computed the average monthly relative reduction on the monthly maximum power at the PCC for 1000 months. The idea behind it is that, if prediction and control errors of n different systems are not correlated, they will achieve better performances, w.r.t. a single one, in the reduction of the monthly peak by means of statistical smoothing. The results are shown in figure 4. The results show that the relative peak reduction starting at around 4% can be reduced by 10% in the case of 5 parallel systems. The peak reduction than reached a plateau at around 14%. Even if this is an optimistic estimation, since in reality forecasting and controller errors won't be uncorrelated, it gives an idea of the performance increase for a group of deterministic controllers performing local peak shaving.

case	cost reduction CHF
ideal	441.68
pilot	37.44

Table 5: Monthly peak costs reduction, in CHF

4.3 Reactive power control

Reactive power control can be used to reduce losses by controlling the ratio of reactive over active power. Although this is a viable and effective strategy to reduce the cost of thermal losses, this option wasn't explored since the controlled batteries didn't have the possibility to accept reactive power set-points.

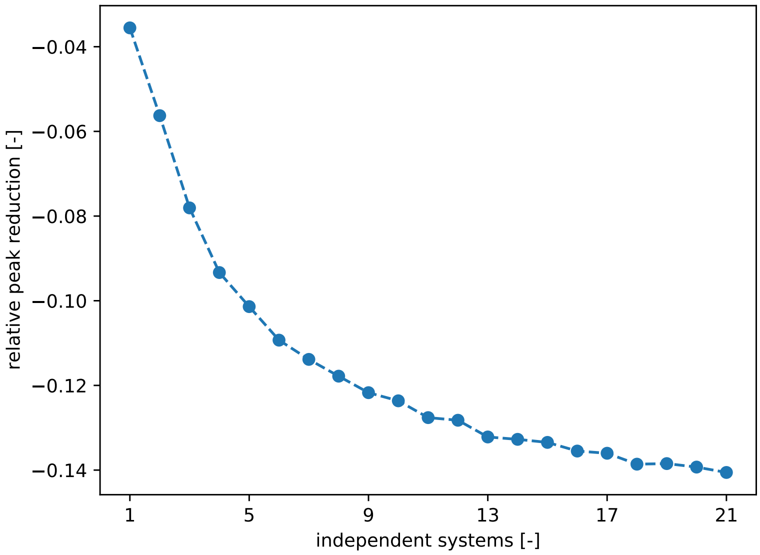

Figure 4: Relative peak reduction considering n independent systems located in n parallel grids. This is the best case result in which the errors of each system can be considered as independent.

5 Discussion

In this deliverable we estimated the cost reduction that can be associated to having operated a battery with a peak shaving objective. The main considered cost reduction is associated to a reduction in the estimated cable and transformer degradation, which has been compared to the cost of replacement/refurbishment of such components. The second term is related to the reduction of the cost associated to the power peak tariff. For the first estimation we must consider that the aging acceleration factor laws strongly depend on the estimated temperature of the components, and that the thermal characteristics of the modeled components weren't fully available at the time of the estimation. Concerning the estimation of power peak tariff, as previously said, this is strongly dependent on the performance of the used forecaster in a given month. In order to better estimate a general performance of the adopted method, we have compared it with a perfect controller and generalized the peak reduction capability to a system of n identical components, using a randomized approach.

References

(1) G. Montanari and L. Simoni, "Aging phenomenology and modeling," *IEEE Transactions on Electrical Insulation*, vol. 28, no. 5, pp. 755–776, Oct. 1993, conference Name: IEEE Transactions on Electrical Insulation.

(2) "Assessing and Managing Cable Ageing in Nuclear Power Plants," Sep. 2016, publisher: IAEA. (Online). Available: https://www.iaea.org/publications/8753/assessing-and-managing-cable-ageing-in-nuclear-power-plants

(3) M. H. Kim, H. J. Seo, S. K. Lee, and M. C. Lee, "Influence of Thermal Aging on the Combustion Characteristics of Cables in Nuclear Power Plants," p. 17, 2021.

(4) V. N. Pugach, D. A. Polyakov, K. I. Nikitin, I. L. Zakharov, and N. N. Petukhova, "Analysis of Temperature Conditions Influence on Cables Insulation Operation Life," *Journal of Physics: Conference Series*, vol. 1260, no. 5, p. 052027, Aug. 2019. (Online). Available: https://iopscience.iop.org/article/10.1088/1742-6596/1260/5/052027

(5) D. D. Evans, "Calculated operating temperatures of thermally insulated electric cables," p. 48.

(6) S. Sachan, R. Wen, Y. Xiang, L. Yao, and C. Zhou, "A Stochastic Electrothermal Degradation Model of Power Cables," p. 10, 2015.

(7) E. Cazacu, V. Ionita, and L. Petrescu, "Thermal Aging of Power Distribution Transformers Operating under Nonlinear and Balanced Load Conditions," *Advances in Electrical and Electronic Engineering*, vol. 16, no. 1, pp. 92 – 100, Apr. 2018. (Online). Available: http://advances.utc.sk/index.php/AEEE/article/view/2701

(8) "IEEE Guide for Loading Mineral-Oil-Immersed Transformers and Step-Voltage Regulators," IEEE, Tech. Rep., iSBN: 9780738171951. (Online). Available: http://ieeexplore.ieee.org/document/6166928/

(9) B. Thormann and T. Kienberger, "Estimation of Grid Reinforcement Costs Triggered by Future Grid Customers: Influence of the Quantification Method (Scaling vs. Large-Scale Simulation) and Coincidence Factors (Single vs. Multiple Application)," *Energies*.